







# Dynamic Pneumococcal Genetic Adaptations Support Bacterial Growth and Inflammation during Coinfection with Influenza

 Amanda P. Smith,<sup>a</sup> Lindey C. Lane,<sup>a</sup> Tim van Opijnen,<sup>b</sup> Stacie Woolard,<sup>c</sup> Robert Carter,<sup>d</sup> Amy Iverson,<sup>e</sup> Corinna Burnham,<sup>e</sup> Peter Vogel,<sup>f</sup> Dana Roeber,<sup>g</sup> Gabrielle Hochu,<sup>a</sup>  Michael D. L. Johnson,<sup>h</sup> Jonathan A. McCullers,<sup>a</sup>  Jason Rosch,<sup>e</sup>  Amber M. Smith<sup>a</sup>

<sup>a</sup>Department of Pediatrics, University of Tennessee Health Science Center, Memphis, Tennessee, USA

<sup>b</sup>Department of Biology, Boston College, Chestnut Hill, Massachusetts, USA

<sup>c</sup>Department of Flow Cytometry, St. Jude Children's Research Hospital, Memphis, Tennessee, USA

<sup>d</sup>Department of Oncology, St. Jude Children's Research Hospital, Memphis, Tennessee, USA

<sup>e</sup>Department of Infectious Diseases, St. Jude Children's Research Hospital, Memphis, Tennessee, USA

<sup>f</sup>Department of Pathology, St. Jude Children's Research Hospital, Memphis, Tennessee, USA

<sup>g</sup>The Hartwell Center, St. Jude Children's Research Hospital, Memphis, Tennessee, USA

<sup>h</sup>Department of Immunobiology, University of Arizona, Tucson, Arizona, USA

**ABSTRACT** *Streptococcus pneumoniae* (pneumococcus) is one of the primary bacterial pathogens that complicates influenza virus infections. These bacterial coinfections increase influenza-associated morbidity and mortality through a number of immunological and viral-mediated mechanisms, but the specific bacterial genes that contribute to postinfluenza pathogenicity are not known. Here, we used genome-wide transposon mutagenesis (Tn-Seq) to reveal bacterial genes that confer improved fitness in influenza virus-infected hosts. The majority of the 32 genes identified are involved in bacterial metabolism, including nucleotide biosynthesis, amino acid biosynthesis, protein translation, and membrane transport. We generated mutants with single-gene deletions (SGD) of five of the genes identified, SPD1414, SPD2047 (*cbiO1*), SPD0058 (*purD*), SPD1098, and SPD0822 (*proB*), to investigate their effects on *in vivo* fitness, disease severity, and host immune responses. The growth of the SGD mutants was slightly attenuated *in vitro* and *in vivo*, but each still grew to high titers in the lungs of mock- and influenza virus-infected hosts. Despite high bacterial loads, mortality was significantly reduced or delayed with all SGD mutants. Time-dependent reductions in pulmonary neutrophils, inflammatory macrophages, and select proinflammatory cytokines and chemokines were also observed. Immunohistochemical staining further revealed altered neutrophil distribution with reduced degeneration in the lungs of influenza virus-SGD mutant-coinfected animals. These studies demonstrate a critical role for specific bacterial genes and for bacterial metabolism in driving virulence and modulating immune function during influenza-associated bacterial pneumonia.

**KEYWORDS** influenza virus, pneumococcus, genetic adaptation, immune response, metabolism, pathogenesis

**B**acterial pathogens often complicate influenza virus infections, causing increased morbidity and mortality, and *Streptococcus pneumoniae* (pneumococcus) is one of the leading pathogens that has presented as a risk factor for hospitalization, severe disease, and mortality during influenza epidemics and pandemics (1–7). There is considerable genetic diversity within and between pneumococcal serotypes, and laboratory and clinical studies suggest that specific strains are preferentially promoted in influenza virus-infected hosts (8–10). Despite the clinical importance of the synergy

**Citation** Smith AP, Lane LC, van Opijnen T, Woolard S, Carter R, Iverson A, Burnham C, Vogel P, Roeber D, Hochu G, Johnson MDL, McCullers JA, Rosch J, Smith AM. 2021. Dynamic pneumococcal genetic adaptations support bacterial growth and inflammation during coinfection with influenza. *Infect Immun* 89:e00023-21. <https://doi.org/10.1128/IAI.00023-21>.

**Editor** Nancy E. Freitag, University of Illinois at Chicago

**Copyright** © 2021 Smith et al. This is an open-access article distributed under the terms of the [Creative Commons Attribution 4.0 International license](https://creativecommons.org/licenses/by/4.0/).

Address correspondence to Jason Rosch, [jason.rosch@stjude.org](mailto:jason.rosch@stjude.org), or Amber M. Smith, [amber.smith@uthsc.edu](mailto:amber.smith@uthsc.edu).

**Received** 12 January 2021

**Returned for modification** 13 February 2021

**Accepted** 7 April 2021

**Accepted manuscript posted online**

19 April 2021

**Published** 16 June 2021

between influenza viruses and pneumococci, a systematic investigation into bacterial factors that contribute to coinfection disease severity has yet to be performed.

During influenza A virus (IAV) coinfection with pneumococcus, bacteria are able to grow rapidly, the viral burden increases, and significant inflammation amasses. The host-pathogen interplay is complex, with numerous factors contributing to pathogen growth and host disease. Several studies have investigated the impact of viral virulence factors (e.g., reduced epithelial integrity, PB1-F2, and viral neuraminidase [NA]), bacterial virulence factors (e.g., bacterial NA, enhanced attachment, and sialic acid catabolism), and host immune responses (e.g., cytokine storm and cell dysfunction and death) on the pathogenicity of bacterial coinfections during influenza virus infection (11–17). The incidence and severity of coinfection is, in part, a function of the detrimental effects that influenza virus infection has on key immune responses (e.g., alveolar macrophage [AM $\Phi$ ] depletion and dysfunction [18–23], neutrophil and inflammatory macrophage dysfunction [23–32], and abundant production of proinflammatory cytokines [12–17, 33]). However, the role that single genes play in pathogenicity during coinfection remains unclear.

Pneumococci, in particular, are highly adaptable, altering their gene expression and metabolic functions to adjust to multiple host niches during infection, and several genes have been identified as regulators of transmissibility and disease severity during primary pneumococcal infection (34–45). Select pneumococcal virulence factors have been investigated in the context of IAV infection (e.g., sialic acid catabolism) (46–49), but systematic genomic screens have not yet been employed to assess pneumococcal adaptations during IAV-pneumococcus coinfection. Genome-wide screens have been used to identify influenza virus-induced changes during *Haemophilus influenzae* coinfection (50), which included changes in purine biosynthesis, amino acid metabolism, iron homeostasis, and cell wall synthesis (50). Genomic screens assessing pneumococcal adaptations of the TIGR4 strain in hosts with sickle cell anemia suggested that genes involved in purine biosynthesis, complement function, and iron acquisition were of importance (51). Given these findings and the similarities in bacterial metabolic adaptations under various host pressures, understanding how bacterial genes influence influenza virus-pneumococcus coinfection is imperative.

Here, we used genome-wide transposon insertion sequencing (Tn-Seq) (52) to investigate all nonessential pneumococcal genes that modulate disease severity and immune responses. Doing so could help establish important species- and strain-dependent and -independent mechanisms amenable to targeting with therapeutics. Our Tn-Seq screen revealed a total of 32 genes, some with known metabolic functions, that confer bacterial fitness during influenza virus-pneumococcus coinfection compared to primary bacterial infection. Interestingly, there were time-dependent differences. To determine how select genes affect pathogenicity and host immune responses, we generated 5 single-gene-deletion (SGD) mutants in pneumococcal strain D39 (D39 $\Delta$ *cbiO1* [SPD2047], D39 $\Delta$ *purD* [SPD0058], D39 $\Delta$ 1414, D39 $\Delta$ 1098, and D39 $\Delta$ *proB* [SPD0822]). Lethality was significantly reduced or eliminated during infection despite high bacterial loads in the lungs and blood. This was concurrent with significant reductions in innate pulmonary immune responses and the development of pneumonia in IAV-infected animals. Taken together, these data indicate a critical role for pneumococcal metabolism in shaping host responses and altering disease severity during postinfluenza bacterial pneumonia.

## RESULTS

### Bacterial adaptations during pneumococcus coinfection with influenza virus.

To identify the pneumococcal factors that increase bacterial fitness during IAV infection, we employed a high-throughput transposon sequencing (Tn-Seq) approach (52). We generated a library of ~50,000 transposon insertion mutants in the type 2 pneumococcal strain D39 and then infected groups of mice with 75 50% tissue culture infectious doses (TCID<sub>50</sub>) of influenza virus A/Puerto Rico/34/8 (PR8) or the mock control (phosphate-buffered saline

**TABLE 1** Pneumococcal genes with significant differential fitness during coinfection with IAV<sup>a</sup>

Locus	Gene	Description	Identified at indicated time point (h pbi)	
			12	24
SPD_0002	<i>dnaN</i>	DNA polymerase III subunit beta	×	
SPD_0052		Phosphoribosylformylglycinamide synthase, putative		×
SPD_0053	<i>purF</i>	Amidophosphoribosyltransferase		×
SPD_0054	<i>purM</i>	Phosphoribosylformylglycinamide cyclo-ligase		×
SPD_0055	<i>purN</i>	Phosphoribosylglycinamide formyltransferase	×	×
SPD_0057	<i>purH</i>	Bifunctional purine biosynthesis protein PurH	×	×
<b>SPD_0058</b>	<b><i>purD</i></b>	<b>Phosphoribosylamine-glycine ligase</b>	×	×
SPD_0059	<i>purE</i>	Phosphoribosylaminoimidazole carboxylase, catalytic subunit	×	×
SPD_0182		Conserved hypothetical protein	×	
SPD_0372		Sodium:alanine symporter	×	×
SPD_0395	<i>efp</i>	Translation elongation factor P		×
SPD_0723	<i>rpiA</i>	Ribose 5-phosphate isomerase A	×	
<b>SPD_0822</b>	<b><i>proB</i></b>	<b>Glutamate 5-kinase</b>		×
SPD_0823	<i>proA</i>	Gamma-glutamyl phosphate reductase		×
SPD_0824	<i>proC</i>	Proline-5-carboxylate reductase		×
SPD_0907	<i>hemK</i>	HemK protein	×	
SPD_0994	<i>ribF</i>	Riboflavin biosynthesis protein RibF	×	
SPD_1087	<i>fhs</i>	Formate-tetrahydrofolate ligase		×
SPD_1090		Membrane protein, putative		×
<b>SPD_1098</b>		<b>Amino acid ABC transporter, amino acid-binding protein/permease protein</b>	×	×
SPD_1099		Amino acid ABC transporter, ATP-binding protein		×
SPD_1130	<i>licD2</i>	Phosphotransferase LicD2		×
SPD_1293		Acetyltransferase, GNAT family protein		×
SPD_1309	<i>pgdA</i>	Peptidoglycan GlcNAc deacetylase		×
SPD_1333		Conserved hypothetical protein		×
SPD_1354		Conserved hypothetical protein	×	
<b>SPD_1414</b>		<b>Oxalate:formate antiporter</b>	×	×
SPD_1468		Phosphoglycerate mutase	×	
SPD_1782	<i>ksgA</i>	Dimethyladenosine transferase	×	
SPD_1923		2,3,4,5-Tetrahydropyridine-2-carboxylate <i>N</i> -succinyltransferase, putative	×	
<b>SPD_2047</b>	<b><i>cbiO1</i></b>	<b>Cobalt ABC transporter, ATP-binding protein CbiO1</b>	×	×
SPD_2048	<i>cbiO2</i>	Cobalt ABC transporter, ATP-binding protein CbiO2		×
Total			17	23

<sup>a</sup>Pneumococcal fitness genes identified at 12 h and 24 h pbi by Tn-Seq during IAV infection compared to mock-infected hosts. Highlighted in boldface are the genes chosen for additional characterization.

[PBS]), followed 7 days later with 10<sup>6</sup> CFU of the transposon library. Bacteria were collected from lungs harvested at 12 h or 24 h post-bacterial infection (pbi), genomic DNA was isolated and sequenced, and the relative abundances and fitness of transposon mutants were calculated (see the supplemental material). Bacterial fitness was first compared pre- and postinfection and then compared between mock- and IAV-infected animals, to identify the differences in genes required for fitness. This analysis highlighted 17 genes at 12 h pbi and 23 genes at 24 h pbi that were required for fitness in IAV-infected hosts (Table 1 and Fig. 1). Of these, 8 genes were detected at both time points. The core set of genes identified at 12 h and 24 h pbi are responsible for amino acid biosynthesis, nucleotide biosynthesis, protein translation, and membrane transport (Fig. 1). Genes in the purine biosynthesis pathway comprised the largest number of genes (8 total: SPD0002 [*dnaN*], SPD0052, SPD0053 [*purF*], SPD0054 [*purM*], SPD0055 [*purN*], SPD0057 [*purH*], SPD0058 [*purD*], and SPD0059 [*purE*]), followed by ATP-binding cassette (ABC) transporters (5 total: SPD1098, SPD1099, SPD2047 [*cbiO1*], SPD2048 [*cbiO2*], and SPD1354 [putative]), protein translation (6 total: SPD0395 [*efp*], SPD1782 [*ksgA*], SPD0907 [*hemK*], SPD1130 [*licD2*], SPD1293, and SPD1923), and proline biosynthesis (3 total: SPD0822 [*proB*], SPD0823 [*proA*], and SPD0824 [*proC*]). Other genes included a putative membrane protein (SPD1090), carbon metabolism (SPD0723 [*rpiA*], SPD1087, SPD1333 [putative], and SPD1468), and riboflavin metabolism (SPD0994).

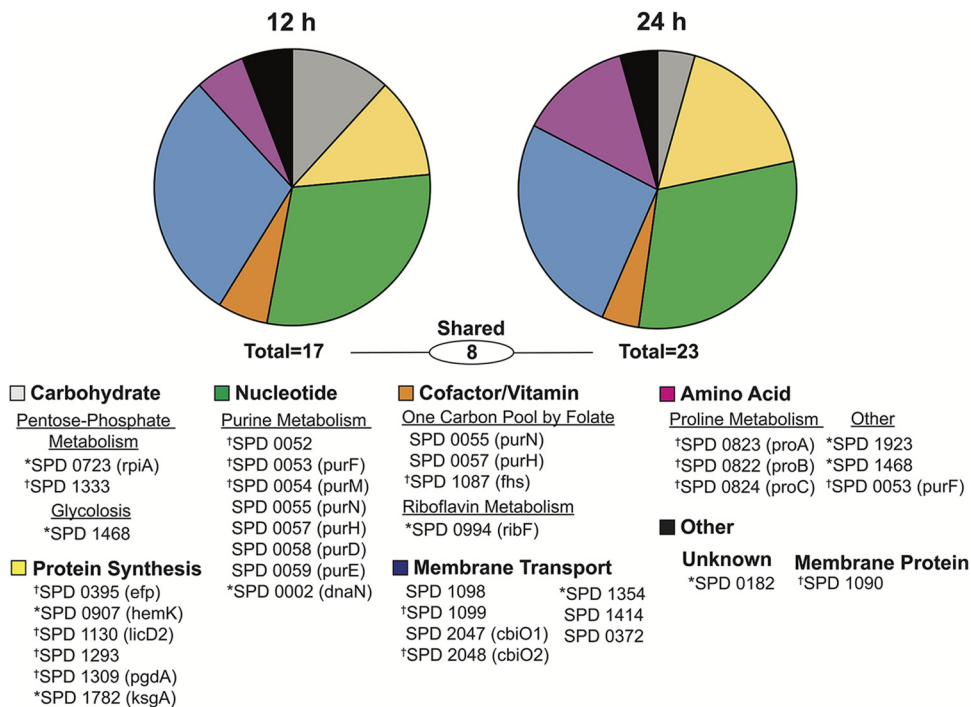


**FIG 1** Time-dependent analysis of pneumococcal genes impacting fitness during influenza virus coinfection. Functional breakdown of the pneumococcal genes that impact bacterial fitness during coinfection with influenza A virus as identified by Tn-Seq. Markers identify genes important only at 12 h pbi\* (17 total) or only at 24 h pbi† (23 total). The absence of a marker indicates significance at both time points (8 total).

**Impaired bacterial metabolism selectively reduces fitness *in vitro*.** We generated single-gene-deletion (SGD) bacterial mutants from 3 of the categories identified (D39Δ*cbiO1*, D39Δ1414, D39Δ1098 [membrane transport], D39Δ*purD* [purine metabolism], and D39Δ*proB* [proline metabolism]) to assess the differential fitness conveyed by genes predicted by Tn-seq (Table 1, Fig. 1, and Table S1). The growth of the SGD mutants in culture medium was unaffected, with the exception of D39Δ*cbiO1*, which was significantly attenuated from 3 h to 8 h ( $P < 0.05$ ) and was the only SGD strain that had not autolysed after 24 h (Fig. 2A). During metabolic starvation (i.e., in PBS), D39Δ1098 decayed more rapidly ( $P = 0.01$ ) and D39Δ*cbiO1* more slowly ( $P < 0.01$ ), but other SGD mutants were similar to the wild type (WT) (Fig. 2B). Bacterial growth was rescued when PBS cultures were supplemented with lung homogenate supernatants (s/n) (Fig. S1A and B in the supplemental material) and was not different than that of the WT strain D39 after 6 h of culture in lung homogenate s/n from mock- or IAV-infected mice (75 TCID<sub>50</sub> PR8, 7 days) (Fig. S1C and D).

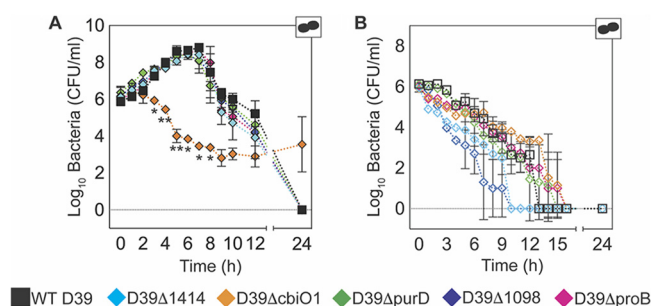


**FIG 2** *In vitro* growth kinetics of SGD mutant bacteria. Bacteria were grown at 37°C in 1 ml of THY medium (A) or PBS (B). \*,  $P < 0.05$ , and \*\*,  $P < 0.01$  (D39Δ*cbiO1* only), for significance compared to WT D39 at the indicated time point (A). Each symbol (squares or diamonds) shows the mean value from two representative experiments, and the bars show the geometric mean values  $\pm$  standard deviations (SD). Cartoons indicate pathogens in the culture (bacteria alone).

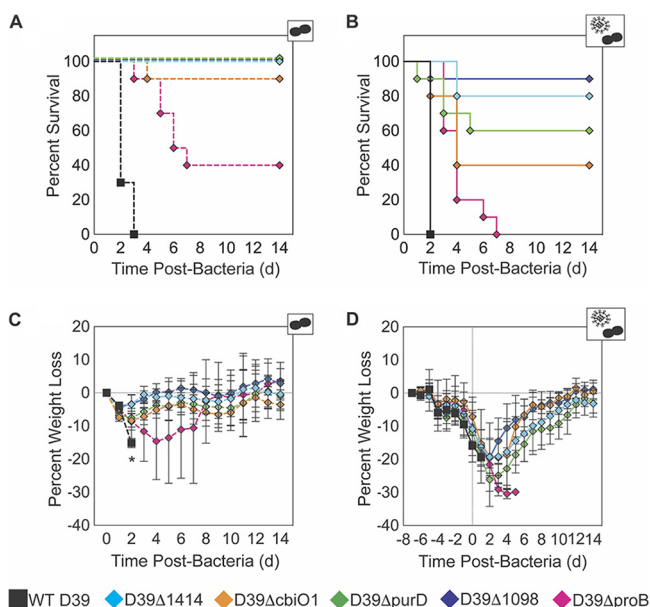


**FIG 3** *In vivo* pathogenicity of infection with SGD mutant bacteria. Kaplan-Meier survival curves (A, B) and weight loss (percent loss compared to naive mice) (C, D) of mice that were mock infected (PBS) (dashed lines; A and C) or IAV infected (75 TCID<sub>50</sub> PR8) (solid lines; B and D), followed 7 days later with 10<sup>6</sup> CFU of the indicated bacteria. Survival curves are significantly different (*P* < 0.01) for each SGD mutant compared to the results for WT D39 in mock-infected (A) and IAV-infected (B) animals. Differences in survival curves are detailed in Table 2. \*, *P* < 0.05, for significant difference in weight loss with each SGD mutant (diamonds) compared to WT D39 (square) at the indicated time point (C). Data are shown as the mean values ± standard deviations (SD) from 10 mice/group. Cartoons indicate infection status of study group (bacteria alone or virus plus bacteria).

**Impaired bacterial metabolism protects against virulence *in vivo*. (i) Mortality is reduced.** To establish the effect of gene deletion on pathogenicity, weight loss was monitored as a measure of disease severity (Fig. 3 and Table 2). In mock- and IAV-infected animals, infection with WT D39 resulted in 100% mortality by 72 h pbi and 48 h pbi, respectively (Fig. 3A and B). In mock-infected animals, mortality was reduced by 90 to 100% with 4 of 5 SGD mutants and by 40% with D39Δ*proB* (all *P* < 0.01) (Fig. 3A and Table 2). Correspondingly, weight loss was significantly reduced (48 h pbi; *P* < 0.05) (Fig. 3C). In IAV-infected animals, mortality was reduced by 40 to 90% with 4 out of 5 SGD mutants (all *P* < 0.01) (Fig. 3B and Table 2). Coinfection with D39Δ*proB* resulted in 100% mortality; however, the mean survival time was lengthened by 5 days (*P* < 0.01) (Fig. 3B and Table 2). In IAV-infected animals, weight loss was not significantly reduced

**TABLE 2** Summary of pathogenicity of SGD mutant bacteria with or without influenza A virus strain PR8 coinfection

Bacterial strain	Log <sub>10</sub> change in <sup>a</sup> :										% survival of mice with indicated treatment <sup>b</sup>	
	Lung bacteria				Blood bacteria				Virus (PR8 + bacteria)		PBS	PR8
	PBS + bacteria		PR8 + bacteria		PBS + bacteria		PR8 + bacteria		4 h	24 h		
4 h	24 h	4 h	24 h	4 h	24 h	4 h	24 h	4 h	24 h			
D39Δ1414	-0.61****	-2.71	-0.94****	-0.83**	-3.79	-5.87	-1.65	<b>-4.97**</b>	0.02	0.43	<b>100****</b>	<b>80****</b>
D39ΔcbiO1	<b>-1.36****</b>	-5.86	<b>-2.05****</b>	<b>-2.11**</b>	-2.31	-6.56	-1.38	<b>-2.35**</b>	0.15	0.29	<b>90****</b>	<b>40***</b>
D39ΔpurD	<b>-0.74****</b>	-0.47	<b>-0.44****</b>	<b>-0.87*</b>	-1.49	-1.28	-0.40	<b>-2.64**</b>	-0.83	0.26	<b>100****</b>	<b>60***</b>
D39Δ1098	<b>-0.59****</b>	-2.17	<b>-0.76****</b>	<b>-0.78**</b>	-3.78	-3.51	-1.69	<b>-2.25**</b>	-0.83	-0.93	<b>100****</b>	<b>90****</b>
D39ΔproB	<b>-1.07****</b>	-1.70	<b>-1.08****</b>	<b>-0.86*</b>	-3.21	-6.56	-1.86	<b>-2.98**</b>	-0.04	-0.19	<b>40****</b>	<b>0****c</b>

<sup>a</sup>Log<sub>10</sub> changes in the levels of lung bacteria, blood bacteria, and lung virus from mice (groups of 5) that were either mock infected (PBS) or IAV infected (75 TCID<sub>50</sub> PR8), followed 7 days later by 10<sup>6</sup> CFU of the indicated bacteria. Comparisons were made between average log<sub>10</sub> bacteria or virus at 4 h pbi and 24 h pbi. Significance in analysis of variance (ANOVA) using a Dunnett correction for multiple comparisons (to WT D39) is indicated by boldface.

<sup>b</sup>Percent increases in survival of animals (groups of 10) that were either mock infected (PBS) or IAV infected (75 TCID<sub>50</sub> PR8), followed 7 days later by 10<sup>6</sup> CFU of the indicated bacteria. Significant differences in Kaplan-Meier survival curves by the log rank test are indicated by boldface. \*, *P* < 0.05; \*\*, *P* < 0.01; \*\*\*, *P* < 0.005; \*\*\*\*, *P* < 0.0001.

<sup>c</sup>Mean survival time at 7 days pbi.

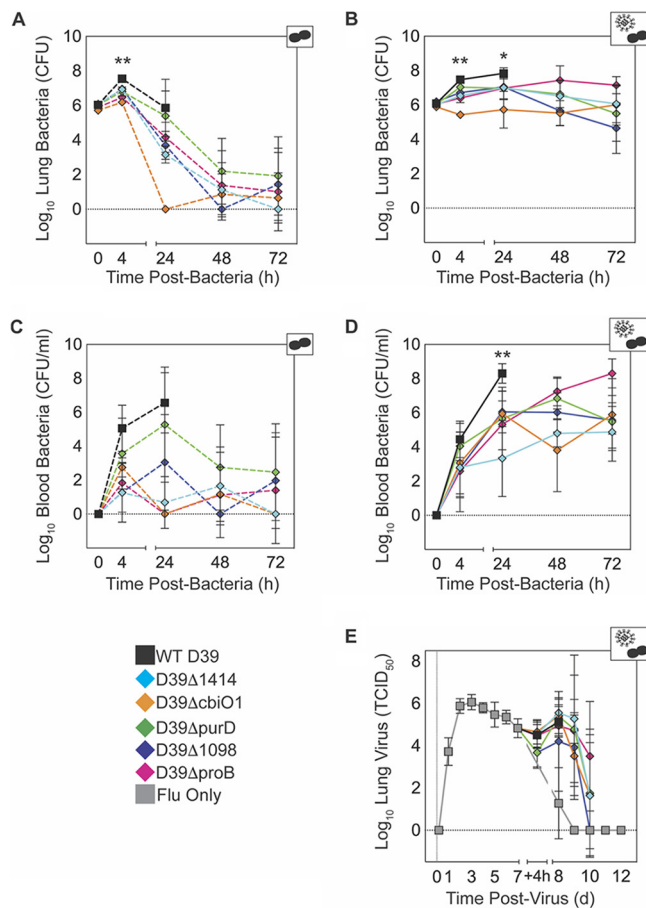


**FIG 4** Viral and bacterial titer kinetics. Lung bacterial titers (A, B), blood bacterial titers (C, D), and lung viral titers (E) from groups of mice either mock infected (PBS) (dashed lines in A and C) or IAV infected ( $75 \text{ TCID}_{50}$  PR8) (solid lines in B, D, and E), followed 7 days later with  $10^6$  CFU of the indicated bacteria. \*,  $P < 0.05$  and \*\*,  $P < 0.01$ , for significance for each of the SGD mutants compared to WT D39 at the indicated time point. Data are shown as the mean values  $\pm$  standard deviations (SD) from 5 mice/group. Cartoons indicate infection status of study group (bacteria alone or virus plus bacteria). The  $\log_{10}$  changes in pathogen loads between each SGD mutant and WT D39 and analysis of variance results are summarized in Table 2.

compared to that of WT D39-infected animals (24 h pbi;  $P > 0.05$ ) (Fig. 3D), and the weights of all SGD-infected animals, except those infected with *D39ΔproB*, began to rebound  $\sim 3$  days pbi and returned to baseline by 12 to 14 days pbi.

**(ii) Bacteria in the lung and blood are reduced.** The lung titer kinetics of the SGD mutants *in vivo* (Fig. 4A and B) mirrored the *in vitro* titer kinetics in lung *s/n*-supplemented cultures (Fig. S2C and D). At 4 h pbi, SGD mutant lung titers were 0.6 to 1.4  $\log_{10}$  CFU lower than those of WT D39 in mock-infected animals and 0.4 to 2.1  $\log_{10}$  CFU lower in IAV-infected animals ( $P < 0.01$ ) (Fig. 4A and B and Table 2). By 24 h pbi, titers were statistically similar and yet reduced compared to those of WT D39 in the lungs (0.5 to 2.7  $\log_{10}$  CFU reduction;  $P > 0.05$ ) and blood (1.3 to 6.6  $\log_{10}$  CFU reduction;  $P > 0.05$ ) of mock-infected animals (Fig. 4A and C and Table 2). However, in IAV-infected animals, SGD mutant titers remained significantly lower in the lungs (0.8 to 2.1  $\log_{10}$  CFU reduction;  $P < 0.05$ ) and blood (2.2 to 5.0  $\log_{10}$  CFU reduction;  $P < 0.01$ ) at 24 h pbi (Fig. 4B and D and Table 2). Despite attenuated growth in the lungs and reduced bacteremia at 24 h pbi, the bacterial loads for each SGD mutant remained high in the lungs and blood of coinfecting animals at 24 h, 48 h, and 72 h pbi (Fig. 4B and D and Table 2).

**(iii) IAV kinetics are similar.** Similar to previous studies (53), viral loads rebounded following coinfection with each SGD mutant bacterial strain. While viral rebound and

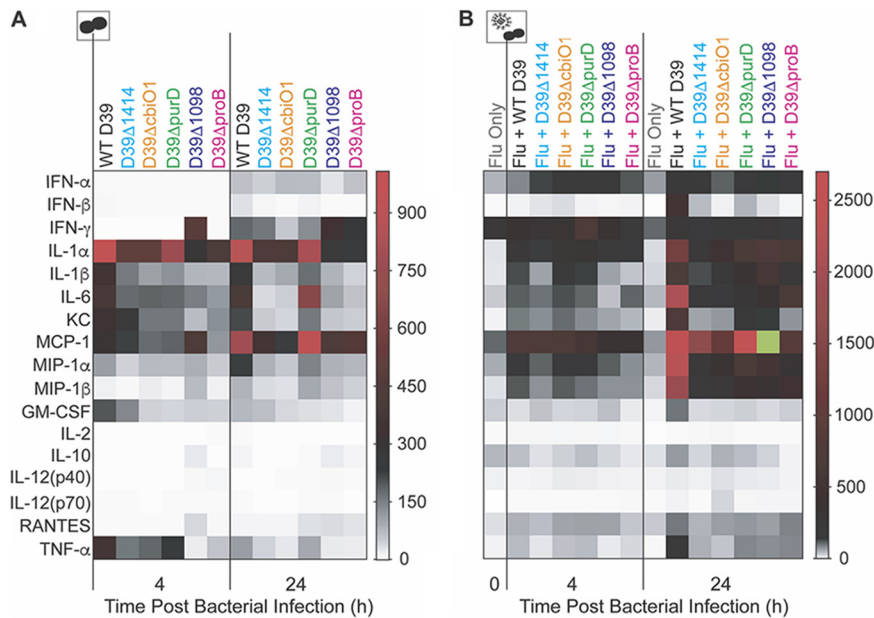


**FIG 5** Heat map of cytokine and chemokine changes. Fold change compared to naive in the mean value of the indicated cytokine/chemokine at 4 h or 24 h pbi in the lungs of mice that were mock infected (PBS) (A) or IAV infected (75 TCID<sub>50</sub> PR8) (B), followed 7 days later with 10<sup>6</sup> CFU of the indicated bacteria. The green square is outside the listed range and indicates a 4,021-fold change. Cartoons indicate infection status of study group (bacteria alone or virus plus bacteria). Plots depicting absolute log<sub>10</sub> picograms (pg) of measured cytokines and chemokines are in Fig. S2 to S4 in the supplemental material.

clearance occurred with various dynamics, each was statistically similar to those found during coinfection with WT D39 ( $P > 0.05$ ) (Fig. 4E and Table 2).

**(iv) Select cytokine and chemokine responses are altered.** To better understand the reduced morbidity and mortality during infection with the SGD mutants, we examined cytokine and chemokine dynamics in the lungs (Fig. 5 and Fig. S2 to S4). In IAV-infected animals, interferon alpha (IFN- $\alpha$ ) and IFN- $\beta$  were significantly reduced at 24 h pbi during infection with SGD mutant bacteria compared to their levels during infection with WT D39 ( $P < 0.05$ ), with the exception of IFN- $\alpha$  during coinfection with D39 $\Delta$ 1414 ( $P = 0.95$ ) and D39 $\Delta$ purD ( $P = 0.17$ ) (Fig. 5 and Fig. S2J and L). Interestingly, at 4 h pbi in IAV-infected animals, IFN- $\alpha$  was elevated in D39 $\Delta$ 1414, D39 $\Delta$ cbiO1, D39 $\Delta$ purD, and D39 $\Delta$ 1098 coinfections ( $P < 0.01$ ) and IFN- $\beta$  was elevated in D39 $\Delta$ cbiO1 coinfection ( $P < 0.01$ ) (Fig. 5 and Fig. S2J and L). In mock-infected animals, IFN- $\alpha$  was unaltered ( $P > 0.05$ ) and IFN- $\beta$  was reduced at 24 h pbi during infection with only D39 $\Delta$ cbiO1, D39 $\Delta$ 1098, and D39 $\Delta$ proB ( $P < 0.05$ ) (Fig. 5 and Fig. S2I and K). At 24 h pbi, interleukin-6 (IL-6), KC, MIP-1 $\beta$ , and granulocyte-macrophage colony-stimulating factor (GM-CSF) were reduced during infection with all SGD mutant bacteria in IAV-infected animals ( $P < 0.05$ ), while only GM-CSF was reduced with D39 $\Delta$ 1098 ( $P < 0.05$ ) and D39 $\Delta$ proB ( $P < 0.01$ ) in mock-infected animals (Fig. 5 and Fig. S2 to S4). IL-1 $\alpha$ , IL-1 $\beta$ , MIP-1 $\alpha$ , and tumor necrosis factor alpha (TNF- $\alpha$ ) were reduced in both IAV- and mock-infected animals at 24 h pbi during infection with each SGD mutant compared to their levels during infection with WT D39 ( $P < 0.05$ ), except for D39 $\Delta$ purD in mock-infected animals ( $P > 0.05$ ) (Fig. 5 and Fig. S2 to S4). Minimal differences were detected for monocyte chemoattractant protein 1 (MCP-1), RANTES, IL-2, IFN- $\gamma$ , IL-10, IL-12(p40), and IL-12(p70), except during primary infection with D39 $\Delta$ 1098 and D39 $\Delta$ proB (Fig. 5 and Fig. S3 and S4). Overall, there were reductions in inflammatory cytokines and chemokines during infection with SGD mutant bacteria compared to their levels during infection with WT D39, and the extent and timing of these reductions differed based on the IAV infection status of the host.

**(v) Inflammatory cell responses are reduced.** In accordance with the changes detected in pulmonary cytokines and chemokines, infection with SGD mutant bacteria

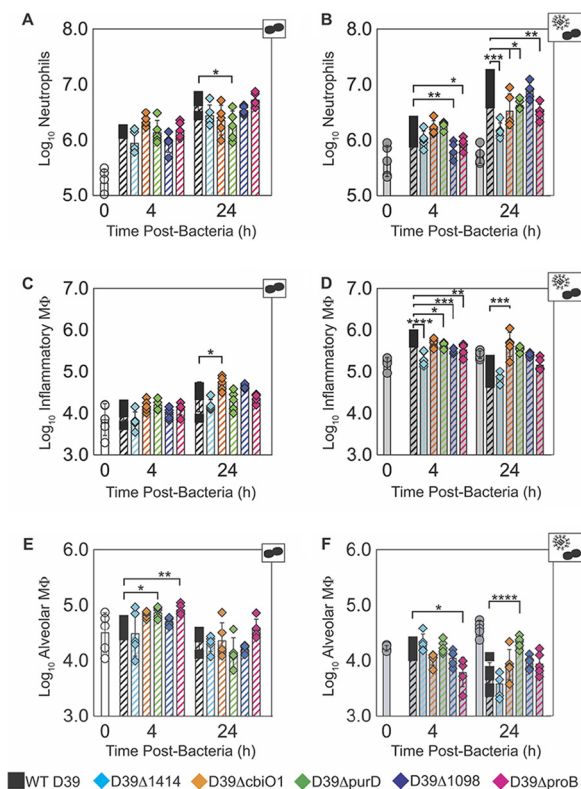


**FIG 6** Pulmonary immune cell kinetics. Kinetics at 4 h or 24 h pbi of neutrophils (A, B), inflammatory macrophages (C, D), and alveolar macrophages (E, F) from mice that were mock infected (PBS) (A, C, E) or IAV infected (75 TCID<sub>50</sub> PR8) (B, D, F), followed 7 days later with 10<sup>6</sup> CFU of the indicated bacteria. Each symbol (circles, squares, or diamonds) represents the value for a single mouse, and the bars show the geometric mean values  $\pm$  standard deviations (SD) from 5 mice/group. Mice were either uninfected (open [white]), infected with IAV only for 7 days ( $t=0$ ) or 8 days ( $t=24$ ) (solid [light gray]), infected with bacteria (open, hatched, colored), or coinfecting with IAV and bacteria (solid, hatched, colored). \*,  $P < 0.05$ ; \*\*,  $P < 0.01$ ; \*\*\*,  $P < 0.005$ ; \*\*\*\*,  $P < 0.0001$ . Cartoons indicate infection status of study group (bacteria alone or virus plus bacteria). The flow cytometry gating scheme is in Fig. S5, and additional cellular dynamics are in Fig. S6.

altered the dynamics of select immune cells in the lungs (Fig. 6 and Fig. S5-S6). In mock-infected animals, neutrophils (Ly6G<sup>hi</sup>) were not different at 4 h pbi during infection with any of the SGD mutants ( $P > 0.05$ ) and were only reduced at 24 h pbi by *D39ΔpurD* ( $P < 0.05$ ) (Fig. 6A). However, in IAV-infected animals, neutrophils were reduced at 4 h pbi with *D39Δ1098* ( $P < 0.01$ ) and *D39ΔproB* ( $P < 0.05$ ) and at 24 h pbi with *D39Δ1414*, *D39ΔcbiO1*, *D39ΔpurD*, and *D39ΔproB* ( $P < 0.05$ ) (Fig. 6B). Inflammatory macrophages (IM $\Phi$ ; Ly6G<sup>-</sup>, CD11c<sup>hi</sup>, F4/80<sup>hi</sup>, CD11b<sup>+</sup>) were also similar at 4 h pbi for all of the SGD mutants in mock-infected animals ( $P > 0.05$ ) and were increased by only *D39ΔcbiO1* infection at 24 h pbi ( $P < 0.05$ ) (Fig. 6C). However, in IAV-infected animals, IM $\Phi$  were reduced at 4 h pbi during infection with *D39Δ1414*, *D39ΔpurD*, *D39Δ1098*, and *D39ΔproB* ( $P < 0.05$ ) (Fig. 6D). *D39ΔcbiO1* did not lead to reduced IM $\Phi$  at 4 h pbi ( $P = 0.14$ ) but did induce an increase in IM $\Phi$  at 24 h pbi ( $P < 0.01$ ) that was not observed with the other SGD mutants (Fig. 6D). There were minimal differences in T cell populations (Fig. S6I to L) or the extent of AM $\Phi$  depletion (Ly6G<sup>-</sup>, CD11c<sup>hi</sup>, F4/80<sup>hi</sup>, CD11b<sup>-</sup>) (Fig. 6E and F) in mock- or IAV-infected animals. Thus, infection with SGD mutant bacteria induced less neutrophil and IM $\Phi$  infiltration in a time-dependent manner in IAV-infected hosts, but these cells were largely unaltered in mock-infected hosts.

**(vi) Pathology and neutrophil degeneration are reduced.** There was extensive pulmonary consolidation at 24 h pbi in the lungs of mice coinfecting with WT D39, as characterized by thickened septa and alveoli filled with a mixture of neutrophils, free bacteria, and proteinaceous exudates (Fig. 7A). These lesions were dramatically reduced during



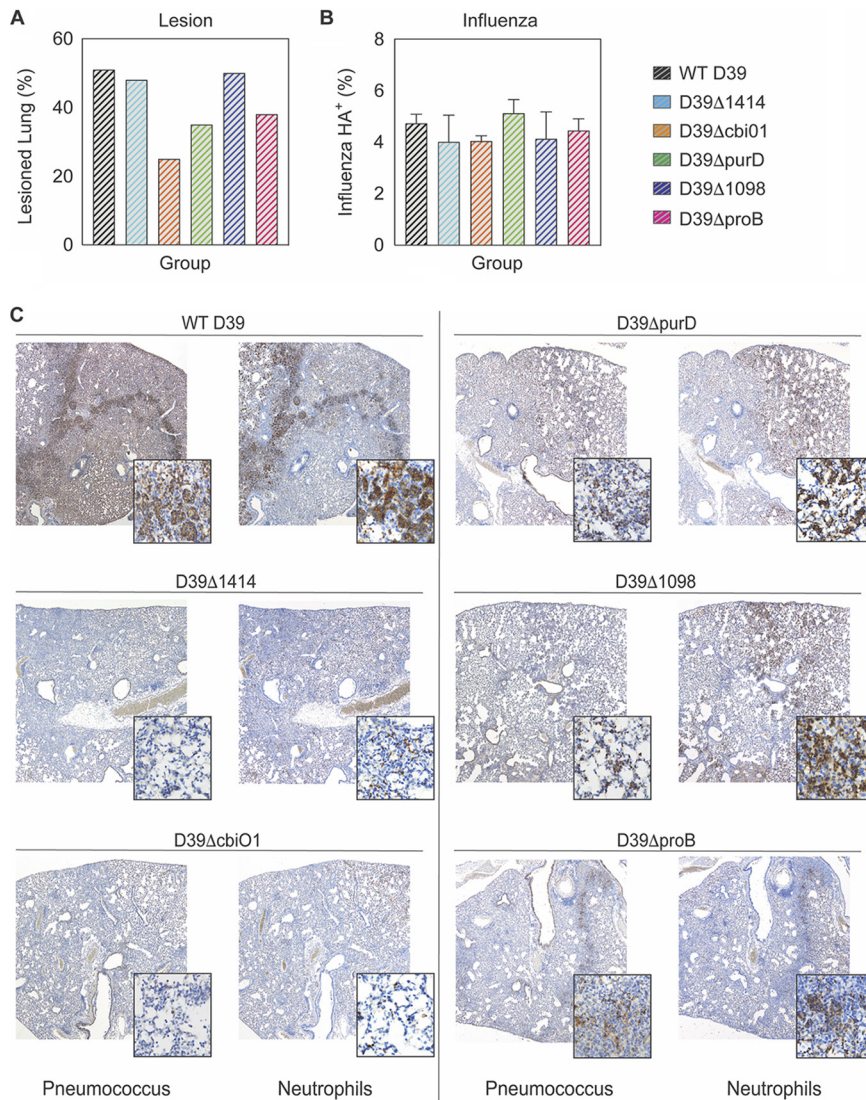


**FIG 7** Lung pathology during IAV-pneumococcus coinfection. Serial sections of lungs at 24 h pbi from mice that were IAV infected (75 TCID<sub>50</sub> PR8), followed 7 days later with 10<sup>6</sup> CFU of the indicated bacteria, were stained with hematoxylin and eosin (HE) for histological analysis (A) or immunohistochemistry (IHC) for influenza virus HA glycoprotein (B), pneumococcus, or neutrophil Ly6G/6C antigen (C). Quantification was performed by a pathologist blinded to the study design (A) or with MIPAR version 3.0 image analysis software (B) (Fig. S7). Bar graphs depict the percent area positive in mice used for representative images (A) or the geometric mean ± standard deviation of sections from 2 mice/group (B). Representative images are at an original ×4 magnification with ×60 magnification insets.

coinfection with D39Δ*proB*, D39Δ*1098*, and D39Δ*1414* and almost absent in D39Δ*cbiO1* and D39Δ*purD* coinfection (Fig. 7A). Immunohistochemical (IHC) staining showed a similar extent of influenza virus antigen (Fig. 7B) but dramatically less bacterial antigen at 24 h pbi during coinfection with each of the SGD mutants (Fig. 7C and Fig. S7A), which mirrored the pulmonary viral and bacterial loads (Fig. 4B and E). In WT D39-coinfected animals, intracellular and extracellular bacterial antigen was present throughout areas showing influenza lesions, including perivascular connective tissues, consolidated alveolar parenchyma, and the central hypocellular area of resolving lesions. Bacterial antigen was not detected in the resolving influenza lesions with any of the SGD mutants, except for D39Δ*1098*, where few bacteria or pneumococcal-antigen-positive macrophages were present. IHC staining also showed massive neutrophil infiltration in WT D39 coinfection (Fig. 7C), and the resolving influenza lesions were consistently surrounded by sharply demarcated hypercellular bands

composed of viable neutrophils and those undergoing hydropic degeneration as noted by a board-certified pathologist. Degenerating neutrophils histologically presented with swollen smudged nuclei undergoing lysis and were often admixed with fibrin, edema fluid, and necrotic cell debris. In contrast, during D39 $\Delta$ *proB*, D39 $\Delta$ *purD*, and D39 $\Delta$ 1098 coinfections, neutrophilic infiltrates generally appeared in clusters within alveoli peripheral to influenza lesions or scattered widely throughout inflamed areas in the lungs. Neutrophil infiltrates in these lungs consisted mostly of intact, nondegenerating cells that formed indistinct bands surrounding the influenza lesions (Fig. 7C). Animals coinfecting with D39 $\Delta$ 1414 and D39 $\Delta$ *cbiO1* had the lowest numbers of neutrophils, which were mostly nondegenerating and scattered throughout inflamed areas (Fig. 7C). Neutrophils were rare or absent within the resolving influenza lesions in animals coinfecting with an SGD mutant.

## DISCUSSION

Pathogenicity during IAV-pneumococcus coinfection is influenced by several pathogen and host factors, including the viral and bacterial strains and doses and the strength of the inflammatory response (11–16). Our study presented here highlights the importance of specific genetic factors in contributing to this pathogenicity and to the dysregulated host response. By using Tn-Seq as an unbiased approach, we identified 32 genes as being critical to pneumococcal survival in the IAV-infected host in a time-dependent manner (Table 1 and Fig. 1). Unsurprisingly, known bacterial virulence genes were not varied in our screen, likely because those factors affect disease equally regardless of viral infection status (40, 41, 43). The genes identified are mostly involved in bacterial metabolism, which supports findings that the lung metabolome is altered during influenza virus infection. Moreover, this selective pressure of the host environment suggests that equivalent bacterial alterations may occur across coinfecting pneumococcal strains and serotypes, but only the D39 strain is assessed herein. Our *in vivo* data suggest that some identified genes function as virulence factors in both mock- and IAV-infected hosts. However, the immunomodulatory effects differed dramatically between healthy mice and those infected with the influenza virus, highlighting the importance of immune and metabolic alterations in the susceptibility to and severity of bacterial coinfection.

Altered metabolic regulation has been observed during murine influenza virus infection (54–57) and *in vitro* influenza virus infection of primary human bronchotracheal epithelial (HBAE) cells (58, 59) and in pediatric patients infected with influenza virus (58). However, even with the knowledge that influenza virus infection induces metabolic changes and that pneumococci modulate metabolic pathways under host-specific pressures (51, 60), the collection of genes identified here was not intuitive, nor was their precise contribution to the infection dynamics. It has been shown that purine metabolic pathways are altered in *Haemophilus influenzae* and pneumococcus (D39 strain) within influenza virus-infected hosts (49, 50) and in pneumococcus (TIGR4 strain) within hosts with sickle cell disease (51). Here, eight genes with roles in purine metabolism were identified, including SPD0058 (*purD*) (Table 1 and Fig. 1) (61–63). This could indicate a common mechanism for bacterial adaptation within inflammatory environments. In influenza virus-infected hosts, purine biosynthesis is upregulated (55) and purine analogs can be used to reduce disease severity (e.g., by the antiviral T-705 [64, 65]). However, the intermediates of purine biosynthesis become depleted following bacterial infection (50), rendering genes of *de novo* purine intermediate synthesis (*purD* and *purC*) critical to coinfecting bacteria (Table 1 and Fig. 1) (50, 51). Here, it is likely that changes in purine scavenging and competition for environmentally available purines/purine intermediates modulate host immune cell function during infection with D39 $\Delta$ *purD*, contributing to decreased lethality (Fig. 3B) and immunopathology (Fig. 7A) in IAV-infected hosts.

Several of the genes identified here act in glutamate/glutamine biosynthesis, which, while important for bacterial pathogenesis in otherwise healthy individuals, plays a key role during influenza virus-pneumococcus coinfection. Here, both genes in the locus pinpointed as the main ABC glutamine/glutamate transporter of pneumococci (SPD1098/1099) (66, 67) were identified in our screen (Table 1 and Fig. 1). Deleting SPD1098 increased

survival by 90% in coinfecting animals (Fig. 3B), despite neutrophil accumulation equivalent to that in WT D39 coinfection (Fig. 6B and Fig. 7C). Genes involved in proline biosynthesis, a process downstream from glutamate metabolism (61–63), were also identified, including SPD0822/SPD0823 (*proB/proA*) (Table 1 and Fig. 1). Deletion of SPD0822 (*proB*) delayed mortality during coinfection (Fig. 3B) and led to reduced neutrophils and IMΦ in influenza virus-infected hosts, but not in mock-infected hosts (Fig. 6). Glutamine is utilized at a high rate by immune cells and is needed for optimal function of macrophages and neutrophils (68–73). Since pulmonary cells have increased dependence on glutamine during influenza virus infection (57, 58), it is probable that competition for limited environmentally available glutamine altered neutrophil infiltration and function, thereby reducing morbidity and mortality in IAV-infected hosts coinfecting with these SGD mutants (Fig. 3B and 5 to 7). Investigating metabolic alterations of innate immune cells during IAV infection would clarify the host-pathogen interactions observed here.

The functions of some genes identified here, including three other ABC transporters (e.g., SPD2047/SPD2048 [*cbiO1/cbiO2*] and SPD1414), are not well characterized. While it is understood that ABC transporters are important for pneumococcal virulence (35, 36, 74–77), investigating the impact of each gene identified in our screen provides insight into respiratory changes that occur during influenza virus infection. The role of cobalt in pneumococcal physiology and virulence remains unclear (78, 79), but the *cbiO* locus (putative cobalt transporter) was previously identified by microarray analysis as necessary for pneumococcal pathogenicity (42). Interestingly, bacteria lacking SPD2047 reach significantly higher lung titers in IAV-infected animals than in mock-infected animals (Fig. 4A to D), suggesting that cobalt metabolism may be modified by influenza virus infection. To our knowledge, no study has assessed cobalt dynamics during influenza. The TIGR4 analog of the oxalate/formate antiporter SPD1414 (SP1587) has been shown to be important for bacterial survival in the lungs and blood (36, 80), cerebrospinal fluid (36), and nasopharynx (80). Here, deletion of SPD1414 reduced lethality (Fig. 3B), neutrophil infiltration, and pulmonary damage in IAV-infected hosts (Fig. 6 and 7). These results indicate roles for cobalt and oxalate/formate in the susceptibility to pneumococcal pneumonia during influenza virus infection.

Mortality during influenza virus-pneumococcus coinfection is typically associated with an exuberant immune response coupled with high pathogen loads in the lung and the blood (14–16, 24, 81–83). However, reduced inflammation can lessen disease severity even with sustained bacterial loads (26). Here, the growth of SGD mutant bacteria in IAV-infected animals was significantly attenuated (0.8 to 2.1 log<sub>10</sub> reduction compared to the growth of WT D39) but not strictly correlated with pathogenicity and insufficient to account for the extreme reductions in mortality (up to 90%) (Fig. 3B and 4 and Table 2), as equivalently reduced bacterial loads of WT D39 in IAV-infected animals still induce significant mortality (Fig. S8). In addition, AMΦ, which dictate the initial pneumococcal invasion and growth kinetics during IAV infection (18–20, 23), are not different during coinfection with most SGD mutants than with WT D39 (Fig. 6F). The contractions of the pulmonary CD8<sup>+</sup> T cells (Fig. S6L) (84) and the rebounds of viral loads (Fig. 4E) were not different during coinfection with SGD mutant bacteria, which supports our previous findings that the mechanisms underlying rapid bacterial growth are independent from those that influence the postbacterial infection viral rebound and pathogenicity (19, 20). These findings suggest that the observed improvements in immune responses and disease outcome are not solely driven by the differences in bacterial loads. Reduced cytokine levels, specifically, lowered type I IFNs (Fig. 5 and Fig. S2J and L), can improve neutrophil function (21, 24, 25, 85–89) and reduce epithelial cell death and lung permeability (90) and, thus, reduce pathogenicity (Fig. 3B, 5, and 7). Moreover, reduced neutrophil infiltration and degeneration (Fig. 6B and 7C) may have mitigated the damaging cytokine storm that is typically associated with IAV-pneumococcus pneumonia (12–17, 33). A direct correlation between survival and any single host immune response in the early stages of coinfection (0 to 24 h pbi) was not readily apparent. It is possible that unmeasured components and/or cumulative effects influence lethality at later time points. These studies underscore the independent nature of pathogen

growth and pathogenicity and illuminate the difficulty in reducing coinfection pathogenicity to a single variable.

Understanding how bacterial adaptations influence the development of pneumonia during influenza virus infections is important to effectively combat the disease. Here, we provide insight into the contribution of specific pneumococcal genes and into the regulatory host-pathogen dynamics that arise during IAV-pneumococcus coinfection. Our findings highlight the critical role of influenza virus-induced metabolic shifts in promoting bacterial infection and altering immune function and suggest that targeting a single pneumococcal gene or metabolite could be an effective intervention to abrogate bacterial pneumonia during influenza virus infection. Further dissecting bacterial adaptations in other pneumococcal serotypes and strains and coinfecting species may help identify therapeutic targets that could be used to prevent or treat postinfluenza bacterial infections.

## MATERIALS AND METHODS

**Ethics statement.** All experimental procedures were performed under protocol O2A-020 approved by the Animal Care and Use Committee at St. Jude Children's Research Hospital under relevant institutional and American Veterinary Medical Association (AVMA) guidelines and were performed in a biosafety level 2 facility that is accredited by the American Association for Laboratory Animal Science (AALAS).

**Mice.** Adult (6-week-old) female BALB/cJ mice were obtained from Jackson Laboratories (Bar Harbor, ME). Mice were housed in groups of 5 in high-temperature 31.2-cm by 23.5-cm by 15.2-cm polycarbonate cages with isolator lids. Rooms used for housing animals were maintained on a 12-h/12-h light/dark cycle at  $22 \pm 2^\circ\text{C}$  with 50% humidity in the biosafety level 2 facility at St. Jude Children's Research Hospital (Memphis, TN). Prior to inclusion in the experiments, mice were allowed at least 7 days to acclimate to the animal facility, such that they were 7 weeks old at the time of infection. Laboratory Autoclavable Rodent Diet (PMI Nutrition International, St. Louis, MO) and autoclaved water were available *ad libitum*. All experiments were performed under an approved protocol and in accordance with the guidelines set forth by the Animal Care and Use Committee at St. Jude Children's Research Hospital.

**Tn-Seq.** Plasmid DNA harboring *magellan6*, a derivative of the Himar1 Mariner transposon, was purified from *Escherichia coli* with the Qiagen mini plasmid preparation kit (Qiagen). Pneumococcal DNA was isolated by phenol-chloroform extraction and ethanol precipitation from an exponentially growing culture in THY medium (30 mg/ml Todd-Hewitt broth powder and 0.2 mg/ml yeast extract). *In vitro*, *magellan6* transposition reactions were carried out with purified MarC9 transposase, 1  $\mu\text{g}$  of pneumococcal target DNA, and 1  $\mu\text{g}$  of *magellan6* plasmid DNA. Reaction mixtures were incubated for 1 h at  $30^\circ\text{C}$ , inactivated for 20 min at  $72^\circ\text{C}$ , ethanol precipitated, and resuspended in gap repair buffer (50 mM Tris [pH 7.8], 10 mM  $\text{MgCl}_2$ , 1 mM dithiothreitol [DTT], 100 nM deoxynucleoside triphosphates [dNTPs] and 50 ng bovine serum albumin [BSA]). Repair of transposition product gaps was performed with *E. coli* DNA ligase overnight at  $16^\circ\text{C}$ . Repaired transposition products were transformed into naturally competent pneumococcal strain D39. The following day, colonies were scraped off tryptic soy agar (TSA) plates supplemented with 3% sheep erythrocytes and 200 mg/ml spectinomycin (TSA-Spec), pooled into libraries of approximately 50,000 transformants/library, split up into multiple starter cultures, and stored at  $-20^\circ\text{C}$ .

**Bacterial fitness by Tn-Seq.** Bacteria were collected from the blood and lungs of each infected mouse at 12 h pbi or 24 h pbi and plated on TSA-Spec plates as indicated below in "Lung and blood harvesting." Later time points could not be examined due to insufficient numbers of surviving mice. Bacteria were incubated for 12 h at  $37^\circ\text{C}$  and then collected in THY medium and centrifuged at  $500 \times g$  and  $4^\circ\text{C}$  for 10 min. The medium supernatant was removed, and the pellets were stored at  $-20^\circ\text{C}$ . Gene identification by Tn-Seq was performed as described previously (51, 52, 80). The samples at each of the three time points (preselection [inoculum  $\{t_1\}$ ] and postselection [after infection, 12 h  $\{t_2\}$  or 24 h  $\{t_3\}$  pbi]) were sequenced in rapid run mode on an Illumina HiSeq 2000 using the primers and cycle conditions in Table S1A. For each insertion, the fitness,  $W_i$ , was calculated by comparing the fold expansion of the mutant relative to the rest of the population with the following equation (91):

$$W_i = \frac{\ln[N_i(t_{2,3})d/N_i(t_1)]}{\ln\{[1 - N_i(t_{2,3})]d/[1 - N_i(t_{2,3})]\}}$$

where the mutant frequencies at time zero and harvest are  $N_i(t_1)$  and  $N_i(t_{2,3})$ , respectively. The expansion factor ( $d$ ) accounts for bacterial growth during library selection. Additional details of the method are included in the supplemental material.

**Infectious agents.** All experiments were done using the mouse-adapted influenza virus A/Puerto Rico/8/34 (H1N1) (PR8) and type 2 pneumococcal strain D39 variants. The transposon mutant library used for infections was generated as described above in "Tn-Seq." To generate the single-gene-deletion (SGD) mutants, genomic DNA was isolated from WT D39 as described above in "Tn-Seq" and used as the template for gene splicing by overhang extension (SOE) PCR (92, 93). In brief, regions flanking the D39 locus targeted for deletion and containing overhangs complementary to the erythromycin (ERM) resistance cassette (*ermB*) (labeled regions A and B) were generated using the primer sets and cycle conditions indicated in Table S1B (EasyA PCR kit [Agilent Tech] and Bio-Rad T100 thermal cycler). Products were purified using the Zymoclean gel DNA recovery kit (Zymo Research), recombined by PCR (TaKaRa PCR kit [Clontech Laboratories])

using the primers and cycle conditions in Table S1C, and transformed into D39. Transformed bacteria were selected after overnight growth on TSA plates containing 1  $\mu\text{g/ml}$  ERM (TSA-ERM). Infection stocks were grown in THY medium containing 1  $\mu\text{g/ml}$  ERM and stored at  $-80^\circ\text{C}$  in 12% glycerol. ERM resistance cassette insertion and target locus deletion were confirmed by PCR with the primer sets in Table S1D.

**Infection experiments.** The viral infectious dose ( $\text{TCID}_{50}$ ) was determined by interpolation using the method of Reed and Muench (94) using serial dilutions of virus on Madin-Darby canine kidney (MDCK) cells. Bacterial infectious doses (CFU) were determined by serial dilutions on TSA (WT), TSA-ERM (SGD mutants), or TSA-Spec (Tn-seq) plates. Frozen stocks of inocula were diluted in sterile PBS and administered intranasally to groups of 5 (for kinetics) or 10 (for bacteria collection and survival) mice lightly anesthetized with 2.5% inhaled isoflurane (Baxter, Deerfield, IL) in a total volume of 100  $\mu\text{l}$  (50  $\mu\text{l}$  per nostril). Mice were inoculated with either PBS or 75  $\text{TCID}_{50}$  PR8 at day zero and then with  $10^6$  CFU of the transposon mutant library, D39, or an SGD mutant (in 100  $\mu\text{l}$ ) 7 days later. This dose of bacteria was chosen to ensure that sufficient amounts of bacteria were recovered in Tn-Seq experiments, and the CFU of each inoculum was confirmed as described above. For bacterial sequencing, 500  $\mu\text{l}$  of the inoculum was plated on TSA-Spec plates (100  $\mu\text{l}/\text{plate}$ ) ( $t_1$  in "Bacterial fitness by Tn-Seq"). Animals were weighed at the onset of infection and each subsequent day to monitor illness and mortality. Mice were euthanized if they became moribund or lost 30% of their starting body weight.

**Lung and blood harvesting.** Mice were euthanized by  $\text{CO}_2$  asphyxiation. For bacterial sequencing, lungs were perfused with 10 ml PBS, aseptically harvested, washed three times in PBS, and placed on ice in 500  $\mu\text{l}$  PBS. The postperfusion fluid (mixture of blood and PBS) was plated immediately on TSA-Spec plates (150  $\mu\text{l}/\text{plate}$ ). Lungs were then enzyme digested with collagenase (1 mg/ml; Sigma) and physically homogenized using a syringe plunger against a 40- $\mu\text{m}$  cell strainer. Cell suspensions were centrifuged at  $500 \times g$  and  $4^\circ\text{C}$  for 7 min, and the supernatant was plated on TSA-spec plates (500  $\mu\text{l}$ ; 100  $\mu\text{l}/\text{plate}$ ). For *in vitro* SGD growth, lungs were homogenized (Omni TH-01 with 5-mm flat blade) and centrifuged at  $500 \times g$  and  $4^\circ\text{C}$  for 7 min. For *in vivo* kinetics, unperfused lungs were enzyme digested with collagenase as described above and supernatants were used to quantify viral titers, bacterial titers, and cytokine/chemokine levels (5 mice/group). Following red blood cell lysis, cells were washed in staining buffer (PBS, 0.01 M HEPES, 5 mM EDTA, and 0.5% bovine serum albumin [BSA]), counted with trypan blue exclusion using a Cell Countess system (Invitrogen, Grand Island, NY), and prepared for flow cytometric analysis as described below.

**In vitro kinetics.** Bacteria were grown at  $37^\circ\text{C}$  in 1.0 ml of THY medium, PBS, or lung homogenate supernatants (s/n). At each time point, 50  $\mu\text{l}$  was removed, serially diluted in PBS, and plated on TSA (WT) or TSA-ERM plates. Bacterial titers were normalized to the total volume. Three biological replicates were performed.

**Lung and blood titers.** For each mouse, viral titers were obtained using serial dilutions on MDCK monolayers, and bacterial titers were obtained using serial dilutions on TSA (WT) or TSA-ERM (SGD mutants) plates.

**Cytokines.** Cytokines and chemokines were measured in lung supernatant by using a Milliplex Luminex assay [GM-CSF, IFN- $\gamma$ , IL-1 $\alpha$ , IL-1 $\beta$ , IL-2, IL-6, IL-10, IL-12(p40), IL-12(p70), KC, MCP-1, MIP-1 $\alpha$ , MIP-1 $\beta$ , RANTES, and TNF- $\alpha$ ] and enzyme-linked immunosorbent assay (ELISA) (IFN- $\alpha$ , $\beta$ ). Prior to use, cell debris and aggregates were removed by centrifugation at  $400 \times g$  and  $4^\circ\text{C}$ . Milliplex magnetic bead cytokine/chemokine plates (Millipore) were prepared according to the manufacturer's instructions. Analysis was done using a Bio-Rad BioPlex (HTF system) and Luminex xPonent software. ELISAs for IFN- $\alpha$  and IFN- $\beta$  (PBL Assay Science) were prepared according to the manufacturer's instructions. Plates were read at 450 nm and analyzed using the website [elisaanalysis.com](http://elisaanalysis.com) (no longer available) and confirmed in Prism v9.1.0. The mean concentrations of duplicate samples were calculated by construction of standard curves using a weighted 5PL and 4PL regression for the Milliplex and ELISA data, respectively. Absolute quantities of each cytokine/chemokine were calculated based on the mean concentrations of replicate samples normalized to the lung supernatant volume collected during tissue processing.

**Flow cytometric analysis.** Flow cytometry (LSRII Fortessa; Becton, Dickinson, San Jose, CA) was performed on single cell suspensions after incubation with 200  $\mu\text{l}$  of a 1:2 dilution of Fc block (human gamma globulin) on ice for 30 min, followed by surface marker staining with anti-mouse antibodies to the following proteins: CD11c (clone N418, eFluor450; eBioscience), CD11b (clone M1/70, Alexa Fluor 700; BD Biosciences), Ly6G (clone 1A8, peridinin chlorophyll protein [PerCp]-Cy5.5; Biolegend), Ly6C (clone HK1.4, allophycocyanin [APC]; eBioscience), F4/80 (clone BM8, phycoerythrin [PE]; eBioscience), CD3e (clone 145-2C11, PE-Cy7 [BD Biosciences] or BV785 [Biolegend]), CD4 (clone RM4-5, PE-Cy5; BD Biosciences), CD8 $\alpha$  (clone 53-6.7, BV605; BD Biosciences), CD49b (clone DX5, APC-Cy7 [Biolegend] or APC-e780 [Affymetrix, Inc.]), and major histocompatibility complex class II (MHC-II) (clone M5/114.15.2, fluorescein isothiocyanate [FITC]; eBioscience). The data were analyzed using FlowJo 10.4.2 (Tree Star, Ashland, OR), where viable cells were gated from a forward scatter/side scatter plot and singlet inclusion. Following neutrophil exclusion (Ly6G<sup>hi</sup>), macrophages (M $\Phi$ ) were gated as CD11c<sup>hi</sup> F4/80<sup>hi</sup>, with alveolar macrophages (AM $\Phi$ ) subgated as CD11b<sup>-</sup> and inflammatory macrophages (IM $\Phi$ ) as CD11b<sup>+</sup>. After macrophage exclusion, T cell populations were gated as CD3e<sup>+</sup> and subgated into CD8 T cells (CD3<sup>+</sup> CD8<sup>+</sup> CD4<sup>-</sup> DX5<sup>-</sup>) and CD4 T cells (CD3<sup>+</sup> CD8<sup>-</sup> CD4<sup>+</sup> DX5<sup>-</sup>). From the CD3e<sup>-</sup> population, natural killer (NK) cells were gated as CD3<sup>-</sup> DX5<sup>+</sup> and dendritic cells (DCs) as CD3<sup>-</sup> DX5<sup>-</sup>. DCs were further gated into three subsets of DCs: CD11c<sup>+</sup> CD11b<sup>-</sup>, CD11c<sup>+</sup> CD11b<sup>+</sup>, and CD11c<sup>-</sup> CD11b<sup>+</sup> (Fig. S5). The expression level of MHC-II was used to confirm the identities and activation of M $\Phi$  and DC subsets. The absolute numbers of cell types were calculated based on viable events analyzed by flow cytometry and normalized to the total number of viable cells per sample.

**Histology.** Mice were euthanized by  $\text{CO}_2$  asphyxiation, and lungs were inflated *in situ* via tracheal infusion with 10% neutral buffered formalin solution (NBF; ThermoFisher Scientific, Waltham, MA), followed by

continued fixation in NBF for at least 2 weeks before being embedded in paraffin, sectioned at 4  $\mu$ m, mounted on positively charged glass slides (Superfrost Plus; Thermo Fisher Scientific, Waltham, MA), and dried at 60°C for 20 min. Tissue sections were stained with hematoxylin and eosin (H&E) or subjected to immunohistochemical (IHC) staining to detect influenza virus antigen, pneumococcus, and neutrophils. For detection of these targets, tissue sections underwent antigen retrieval in a prediluted cell conditioning solution (CC1) (catalog number 950-124; Ventana Medical Systems, Indianapolis, IN) for 32 min on a Discovery ultra immunostainer (Ventana Medical Systems, Tucson, AZ). Primary antibodies included (i) a polyclonal goat antibody raised against the hemagglutinin (HA) glycoprotein of B/Florida/04/2006 (Yamagata lineage) influenza virus diluted 1:2,000 (catalog number I7650-05G; US Biologicals, Swampscott, MA), (ii) a rabbit polyclonal antibody to *Streptococcus pneumoniae* diluted 1:1,000 (catalog number NB100-64502; Novus Biologicals, Littleton, CO), and (iii) a rat monoclonal antibody to neutrophils (Ly6G6C) diluted 1:50 (catalog number NB600-1387; Novus Biologicals, Littleton, CO). Binding was detected using OmniMap anti-goat (#760-4647), anti-rabbit (#760-4311), and anti-rat (#760-4457) secondary antibody-horseradish peroxidase (HRP), respectively (Ventana Medical Systems), with the Discovery ChromoMap 3,3'-diaminobenzidine (DAB) kit (Ventana Medical Systems) as the chromogenic substrate. Stained sections were examined by a pathologist (P.V.) who was blind to the experimental group assignments. IHC data were quantified (A.P.S.) using the immunohistochemistry recipe number L006-02 provided in MIPAR, version 3.0.

**Statistical analysis.** Significant differences in Kaplan-Meier survival curves were calculated using the log rank test. *In vitro* growth/decay rates were analyzed by nonlinear regression of log<sub>10</sub> values, and linear slopes were compared by analysis of covariance (ANCOVA). The remainder of the statistical analyses were performed on linear values. Unpaired *t* tests were done to analyze *in vitro* growth dynamics in THY medium and lung cultures. Analyses of variance (ANOVA) were performed using a Dunnett correction for multiple comparisons (to WT D39) to analyze *in vivo* differences, including lung and blood bacterial loads, viral loads, immune cells, cytokines, and chemokines (GraphPad Prism 7.0c). The confidence interval of significance was set to 95%, and *P* values of less than 0.05 were considered significant.

**Data availability.** Illumina sequence reads have been deposited in the NCBI Sequence Read Archive (<http://www.ncbi.nlm.nih.gov/sra>) under accession number PRJNA727261.

## SUPPLEMENTAL MATERIAL

Supplemental material is available online only.

**SUPPLEMENTAL FILE 1**, PDF file, 10.7 MB.

## ACKNOWLEDGMENTS

This work was supported by NIH grants number AI100946, AI125324, and AI139088 (A.M.S.), PATRIC DBP (A.M.S., J.R., J.A.M.), ALSAC (A.P.S., L.C.L., S.W., R.C., A.I., C.B., P.V., D.R., M.D.L.J., J.A.M., J.R.), NIH grant number R25CA23944 (G.H.), and NIH grants number R01AI110724, U01AI124302, and R21AI117247 (T.V.O.).

A.M.S., J.A.M., and J.R. conceived the experiments. A.M.S., A.I., C.B., and M.D.L.J. generated the mutant libraries. D.R., R.C., and T.V.O. completed the sequence analyses. A.P.S. and L.C.L. generated SGD mutant bacteria. A.M.S., A.P.S., L.C.L., and M.D.L.J. performed *in vitro/in vivo* experiments. A.M.S., A.P.S., L.C.L., and G.H. performed the data analysis. P.V. performed the histological analysis. A.M.S. and A.P.S. wrote the manuscript.

## REFERENCES

- Morens DM, Taubenberger JK, Fauci AS. 2008. Predominant role of bacterial pneumonia as a cause of death in pandemic influenza: implications for pandemic influenza preparedness. *J Infect Dis* 198:962–970. <https://doi.org/10.1086/591708>.
- Gill JR, Sheng Z-M, Ely SF, Guinee DG, Beasley MB, Suh J, Deshpande C, Mollura DJ, Morens DM, Bray M, Travis WD, Taubenberger JK. 2010. Pulmonary pathologic findings of fatal 2009 pandemic influenza A/H1N1 viral infections. *Arch Pathol Lab Med* 134:235–243. <https://doi.org/10.1043/1543-2165-134.2.235>.
- Weinberger DM, Simonsen L, Jordan R, Steiner C, Miller M, Viboud C. 2012. Impact of the 2009 influenza pandemic on pneumococcal pneumonia hospitalizations in the United States. *J Infect Dis* 205:458–465. <https://doi.org/10.1093/infdis/jir749>.
- Louria DB, Blumenfeld HL, Ellis JT, Kilbourne ED, Rogers DE. 1959. Studies on influenza in the pandemic of 1957–1958. II. Pulmonary complications of influenza. *J Clin Invest* 38:213–265. <https://doi.org/10.1172/JCI103791>.
- Brundage JF, Shanks GD. 2008. Deaths from bacterial pneumonia during 1918–19 influenza pandemic. *Emerg Infect Dis* 14:1193–1199. <https://doi.org/10.3201/eid1408.071313>.
- Klugman KP, Chien Y-W, Madhi SA. 2009. Pneumococcal pneumonia and influenza: a deadly combination. *Vaccine* 27:C9–C14. <https://doi.org/10.1016/j.vaccine.2009.06.007>.
- Morens DM, Taubenberger JK, Fauci AS. 2009. The persistent legacy of the 1918 influenza virus. *N Engl J Med* 361:225–229. <https://doi.org/10.1056/NEJMp0904819>.
- Gillet Y, Vanhems P, Lina G, Bes M, Vandenesch F, Floret D, Etienne J. 2007. Factors predicting mortality in necrotizing community-acquired pneumonia caused by *Staphylococcus aureus* containing Pantone-Valentine leukocidin. *Clin Infect Dis* 45:315–321. <https://doi.org/10.1086/519263>.
- Iverson AR, Boyd KL, McAuley JL, Plano LR, Hart ME, McCullers JA. 2011. Influenza virus primes mice for pneumonia from *Staphylococcus aureus*. *J Infect Dis* 203:880–888. <https://doi.org/10.1093/infdis/jiq113>.
- McCullers JA, McAuley JL, Browall S, Iverson AR, Boyd KL, Henriques Normark B. 2010. Influenza enhances susceptibility to natural acquisition of and disease due to *Streptococcus pneumoniae* in ferrets. *J Infect Dis* 202:1287–1295. <https://doi.org/10.1086/656333>.
- Smith AM, McCullers JA. 2014. Secondary bacterial infections in influenza virus infection pathogenesis. *Curr Top Microbiol Immunol* 385:327–356. [https://doi.org/10.1007/82\\_2014\\_394](https://doi.org/10.1007/82_2014_394).
- McCullers JA. 2014. The co-pathogenesis of influenza viruses with bacteria in the lung. *Nat Rev Microbiol* 12:252–262. <https://doi.org/10.1038/nrmicro3231>.

13. Short KR, Habets MN, Hermans PWM, Diavatopoulos DA. 2012. Interactions between *Streptococcus pneumoniae* and influenza virus: a mutually beneficial relationship? *Future Microbiol* 7:609–624. <https://doi.org/10.2217/fmb.12.29>.
14. Rynda-Apple A, Robinson KM, Alcorn JF. 2015. Influenza and bacterial superinfection: illuminating the immunologic mechanisms of disease. *Infect Immun* 83:3764–3770. <https://doi.org/10.1128/IAI.00298-15>.
15. Metzger DW, Sun K. 2013. Immune dysfunction and bacterial coinfections following influenza. *J Immunol* 191:2047–2052. <https://doi.org/10.4049/jimmunol.1301152>.
16. Robinson KM, Kolls JK, Alcorn JF. 2015. The immunology of influenza virus-associated bacterial pneumonia. *Curr Opin Immunol* 34:59–67. <https://doi.org/10.1016/j.coi.2015.02.002>.
17. Kash JC, Taubenberger JK. 2015. The role of viral, host, and secondary bacterial factors in influenza pathogenesis. *Am J Pathol* 185:1528–1536. <https://doi.org/10.1016/j.ajpath.2014.08.030>.
18. Ghoneim HE, Thomas PG, McCullers JA. 2013. Depletion of alveolar macrophages during influenza infection facilitates bacterial superinfections. *J Immunol* 191:1250–1259. <https://doi.org/10.4049/jimmunol.1300014>.
19. Smith AM, Adler FR, Ribeiro RM, Gutenkunst RN, McAuley JL, McCullers JA, Perelson AS. 2013. Kinetics of coinfection with influenza A virus and *Streptococcus pneumoniae*. *PLoS Pathog* 9:e1003238. <https://doi.org/10.1371/journal.ppat.1003238>.
20. Smith AM, Smith AP. 2016. A critical, nonlinear threshold dictates bacterial invasion and initial kinetics during influenza. *Sci Rep* 6:38703. <https://doi.org/10.1038/srep38703>.
21. Sun K, Metzger DW. 2008. Inhibition of pulmonary antibacterial defense by interferon- $\gamma$  during recovery from influenza infection. *Nat Med* 14:558–564. <https://doi.org/10.1038/nm1765>.
22. Janssen WJ, Barthel L, Muldrow A, Oberley-Deegan RE, Kearns MT, Jakubzick C, Henson PM. 2011. Fas determines differential fates of resident and recruited macrophages during resolution of acute lung injury. *Am J Respir Crit Care Med* 184:547–560. <https://doi.org/10.1164/rccm.201011-1891OC>.
23. Califano D, Furuya Y, Metzger DW. 2018. Effects of influenza on alveolar macrophage viability are dependent on mouse genetic strain. *J Immunology* 201:134–144. <https://doi.org/10.4049/jimmunol.1701406>.
24. Shahangian A, Chow EK, Tian X, Kang JR, Ghaffari A, Liu SY, Belperio JA, Cheng G, Deng JC. 2009. Type I IFNs mediate development of postinfluenza bacterial pneumonia in mice. *J Clin Invest* 119:1910–1920. <https://doi.org/10.1172/JCI35412>.
25. Tian X, Xu F, Lung WY, Meyerson C, Ghaffari AA, Cheng G, Deng JC. 2012. Poly I:C enhances susceptibility to secondary pulmonary infections by gram-positive bacteria. *PLoS One* 7:e41879. <https://doi.org/10.1371/journal.pone.0041879>.
26. Karlström Å, Heston SM, Boyd KL, Tuomanen EI, McCullers JA. 2011. Toll-like receptor 2 mediates fatal immunopathology in mice during treatment of secondary pneumococcal pneumonia following influenza. *J Infect Dis* 204:1358–1366. <https://doi.org/10.1093/infdis/jir522>.
27. McNamee LA, Harmsen AG. 2006. Both influenza-induced neutrophil dysfunction and neutrophil-independent mechanisms contribute to increased susceptibility to a secondary *Streptococcus pneumoniae* infection. *Infect Immun* 74:6707–6721. <https://doi.org/10.1128/IAI.00789-06>.
28. LeVine AM, Koenigsnecht V, Stark JM. 2001. Decreased pulmonary clearance of *S. pneumoniae* following influenza A infection in mice. *J Virol Methods* 94:173–186. [https://doi.org/10.1016/S0166-0934\(01\)00287-7](https://doi.org/10.1016/S0166-0934(01)00287-7).
29. Sun K, Metzger DW. 2014. Influenza infection suppresses NADPH oxidase-dependent phagocytic bacterial clearance and enhances susceptibility to secondary methicillin-resistant *Staphylococcus aureus* infection. *J Immunol* 192:3301–3307. <https://doi.org/10.4049/jimmunol.1303049>.
30. Abramson JS, Mills EL, Giebink GS, Quie PG. 1982. Depression of monocyte and polymorphonuclear leukocyte oxidative metabolism and bactericidal capacity by influenza A virus. *Infect Immun* 35:350–355. <https://doi.org/10.1128/IAI.35.1.350-355.1982>.
31. Abramson JS, Lewis JC, Lyles DS, Heller KA, Mills EL, Bass DA. 1982. Inhibition of neutrophil lysosome-phagosome fusion associated with influenza virus infection in vitro. Role in depressed bactericidal activity. *J Clin Invest* 69:1393–1397. <https://doi.org/10.1172/jci110580>.
32. Bansal S, Yajjala VK, Bauer C, Sun K. 2018. IL-1 signaling prevents alveolar macrophage depletion during influenza and *Streptococcus pneumoniae* coinfection. *J Immunol* 200:1425–1433. <https://doi.org/10.4049/jimmunol.1700210>.
33. Rudd JM, Ashar HK, Chow VT, Teluguakula N. 2016. Lethal synergism between influenza and *Streptococcus pneumoniae*. *J Infect Public Dis* 2:10.16966/2470-3176.114. <https://doi.org/10.16966/2470-3176.114>.
34. Rowe HM, Karlsson E, Echlin H, Chang TC, Wang L, van Opijnen T, Pounds SB, Schultz-Cherry S, Rosch JW. 2019. Bacterial factors required for transmission of *Streptococcus pneumoniae* in mammalian hosts. *Cell Host Microbe* 25:884–891.e6. <https://doi.org/10.1016/j.chom.2019.04.012>.
35. Tettelin H. 2001. Complete genome sequence of a virulent isolate of *Streptococcus pneumoniae*. *Science* 293:498–506. <https://doi.org/10.1126/science.1061217>.
36. Orihuela CJ, Radin JN, Sublett JE, Gao G, Kaushal D, Tuomanen EI. 2004. Microarray analysis of pneumococcal gene expression during invasive disease. *Infect Immun* 72:5582–5596. <https://doi.org/10.1128/IAI.72.10.5582-5596.2004>.
37. Ogunniyi AD, Giammarinaro P, Paton JC. 2002. The genes encoding virulence-associated proteins and the capsule of *Streptococcus pneumoniae* are upregulated and differentially expressed in vivo. *Microbiology (Reading)* 148:2045–2053. <https://doi.org/10.1099/00221287-148-7-2045>.
38. LeMessurier KS, Ogunniyi AD, Paton JC. 2006. Differential expression of key pneumococcal virulence genes in vivo. *Microbiology (Reading)* 152:305–311. <https://doi.org/10.1099/mic.0.28438-0>.
39. Mahdi LK, Ogunniyi AD, LeMessurier KS, Paton JC. 2008. Pneumococcal virulence gene expression and host cytokine profiles during pathogenesis of invasive disease. *Infect Immun* 76:646–657. <https://doi.org/10.1128/IAI.01161-07>.
40. Kadioglu A, Weiser JN, Paton JC, Andrew PW. 2008. The role of *Streptococcus pneumoniae* virulence factors in host respiratory colonization and disease. *Nat Rev Microbiol* 6:288–301. <https://doi.org/10.1038/nrmicro1871>.
41. Mitchell AM, Mitchell TJ. 2010. *Streptococcus pneumoniae*: virulence factors and variation. *Clin Microbiol Infect* 16:411–418. <https://doi.org/10.1111/j.1469-0691.2010.03183.x>.
42. Ogunniyi AD, Mahdi LK, Trappetti C, Verhoeven N, Mermans D, Van der Hoek MB, Plumtree CD, Paton JC. 2012. Identification of genes that contribute to the pathogenesis of invasive pneumococcal disease by in vivo transcriptomic analysis. *Infect Immun* 80:3268–3278. <https://doi.org/10.1128/IAI.00295-12>.
43. Henriques-Normark B, Tuomanen EI. 2013. The pneumococcus: epidemiology, microbiology, and pathogenesis. *Cold Spring Harb Perspect Med* 3:a010215. <https://doi.org/10.1101/cshperspect.a010215>.
44. Molzen TE, Burghout P, Bootsma HJ, Brandt CT, van der Gaast-de Jongh CE, Eleveld MJ, Verbeek MM, Frimodt-Moller N, Ostergaard C, Hermans PW. 2011. Genome-wide identification of *Streptococcus pneumoniae* genes essential for bacterial replication during experimental meningitis. *Infect Immun* 79:288–297. <https://doi.org/10.1128/IAI.00631-10>.
45. D’Mello A, Riegler AN, Martinez E, Beno SM, Ricketts TD, Foxman EF, Orihuela CJ, Tettelin H. 2020. An in vivo atlas of host-pathogen transcriptomes during *Streptococcus pneumoniae* colonization and disease. *Proc Natl Acad Sci U S A* 117:33507–33518. <https://doi.org/10.1073/pnas.2010428117>.
46. Siegel SJ, Roche AM, Weiser JN. 2014. Influenza promotes pneumococcal growth during coinfection by providing host sialylated substrates as a nutrient source. *Cell Host Microbe* 16:55–67. <https://doi.org/10.1016/j.chom.2014.06.005>.
47. Peltola VT, Murti KG, McCullers JA. 2005. Influenza virus neuraminidase contributes to secondary bacterial pneumonia. *J Infect Dis* 192:249–257. <https://doi.org/10.1086/430954>.
48. McCullers JA, Bartmess KC. 2003. Role of neuraminidase in lethal synergism between influenza virus and *Streptococcus pneumoniae*. *J Infect Dis* 187:1000–1009. <https://doi.org/10.1086/368163>.
49. Liu X, Kimmey JM, Matarazzo L, de Bakker V, Van Maele L, Sirard JC, Nizet V, Veening JW. 2020. Exploration of bacterial bottlenecks and *Streptococcus pneumoniae* pathogenesis by CRISPRi-Seq. *Cell Host Microbe* 29:107–120.e6. <https://doi.org/10.1016/j.chom.2020.10.001>.
50. Wong SM, Bernui M, Shen H, Akerley BJ. 2013. Genome-wide fitness profiling reveals adaptations required by *Haemophilus* in coinfection with influenza A virus in the murine lung. *Proc Natl Acad Sci U S A* 110:15413–15418. <https://doi.org/10.1073/pnas.1311217110>.
51. Carter R, Wolf J, van Opijnen T, Muller M, Obert C, Burnham C, Mann B, Li Y, Hayden Randall T, Pestina T, Persons D, Camilli A, Flynn PM, Tuomanen EI, Rosch JW. 2014. Genomic analyses of pneumococci from children with sickle cell disease expose host-specific bacterial adaptations and deficits in current interventions. *Cell Host Microbe* 15:587–599. <https://doi.org/10.1016/j.chom.2014.04.005>.

52. van Opijnen T, Bodi KL, Camilli A. 2009. Tn-seq: high-throughput parallel sequencing for fitness and genetic interaction studies in microorganisms. *Nat Methods* 6:767–772. <https://doi.org/10.1038/nmeth.1377>.
53. Smith AM. 2018. Host-pathogen kinetics during influenza infection and coinfection: insights from predictive modeling. *Immunol Rev* 285:97–112. <https://doi.org/10.1111/immr.12692>.
54. Milner JJ, Wang J, Sheridan PA, Ebbels T, Beck MA, Saric J. 2014. 1H NMR-based profiling reveals differential immune-metabolic networks during influenza virus infection in obese mice. *PLoS One* 9:e97238. <https://doi.org/10.1371/journal.pone.0097238>.
55. Chandler JD, Hu X, Ko E-J, Park S, Lee Y-T, Orr M, Fernandes J, Uppal K, Kang S-M, Jones DP, Go Y-M. 2016. Metabolic pathways of lung inflammation revealed by high-resolution metabolomics (HRM) of H1N1 influenza virus infection in mice. *Am J Physiol Regul Integr Comp Physiol* 311:R906–R916. <https://doi.org/10.1152/ajpregu.00298.2016>.
56. Cui L, Zheng D, Lee YH, Chan TK, Kumar Y, Ho WE, Chen JZ, Tannenbaum SR, Ong CN. 2016. Metabolomics investigation reveals metabolite mediators associated with acute lung injury and repair in a murine model of influenza pneumonia. *Sci Rep* 6:26076. <https://doi.org/10.1038/srep26076>.
57. Rezinciuc S, Bezavada L, Bahadoran A, Duan S, Wang R, Lopez-Ferrer D, Zink EE, Finklestein D, Green DR, Pasa-Tolic L, Thomas PG, Smallwood HS. 2020. Dynamic metabolic reprogramming in dendritic cells: an early response to influenza infection that is essential for effector function. *bioRxiv* <https://doi.org/10.1101/2020.01.14.906826>.
58. Smallwood HS, Duan S, Morfouace M, Rezinciuc S, Shulkin BL, Shelat A, Zink EE, Milasta S, Bajracharya R, Oluwaseun AJ, Roussel MF, Green DR, Pasa-Tolic L, Thomas PG. 2017. Targeting metabolic reprogramming by influenza infection for therapeutic intervention. *Cell Rep* 19:1640–1653. <https://doi.org/10.1016/j.celrep.2017.04.039>.
59. Kroeker AL, Ezzati P, Coombs KM, Halayko AJ. 2013. Influenza A infection of primary human airway epithelial cells up-regulates proteins related to purine metabolism and ubiquitin-related signaling. *J Proteome Res* 12:3139–3151. <https://doi.org/10.1021/pr400464p>.
60. Syk A, Norman M, Fernebro J, Gallotta M, Farmand S, Sandgren A, Normark S, Henriques-Normark B. 2014. Emergence of hypervirulent mutants resistant to early clearance during systemic serotype 1 pneumococcal infection in mice and humans. *J Infect Dis* 210:4–13. <https://doi.org/10.1093/infdis/jiu038>.
61. Kanehisa M, Furumichi M, Tanabe M, Sato Y, Morishima K. 2017. KEGG: new perspectives on genomes, pathways, diseases and drugs. *Nucleic Acids Res* 45:D353–D361. <https://doi.org/10.1093/nar/gkw1092>.
62. Kanehisa M, Goto S. 2000. KEGG: Kyoto Encyclopedia of Genes and Genomes. *Nucleic Acids Res* 28:27–30. <https://doi.org/10.1093/nar/28.1.27>.
63. Kanehisa M, Sato Y, Kawashima M, Furumichi M, Tanabe M. 2016. KEGG as a reference resource for gene and protein annotation. *Nucleic Acids Res* 44:D457–D462. <https://doi.org/10.1093/nar/gkv1070>.
64. Furuta Y, Takahashi K, Kuno-Maekawa M, Sangawa H, Uehara S, Kozaki K, Nomura N, Egawa H, Shiraki K. 2005. Mechanism of action of T-705 against influenza virus. *Antimicrob Agents Chemother* 49:981–986. <https://doi.org/10.1128/AAC.49.3.981-986.2005>.
65. Kiso M, Takahashi K, Sakai-Tagawa Y, Shinya K, Sakabe S, Le QM, Ozawa M, Furuta Y, Kawaoka Y. 2010. T-705 (favipiravir) activity against lethal H5N1 influenza A viruses. *Proc Natl Acad Sci U S A* 107:882–887. <https://doi.org/10.1073/pnas.0909603107>.
66. Kloosterman TG, Hendriksen WT, Bijlsma JJE, Bootsma HJ, van Hijum SAFT, Kok J, Hermans PWM, Kuipers OP. 2006. Regulation of glutamine and glutamate metabolism by GlnR and GlnA in *Streptococcus pneumoniae*. *J Biol Chem* 281:25097–25109. <https://doi.org/10.1074/jbc.M601661200>.
67. Härtel T, Klein M, Koedel U, Rohde M, Petruschka L, Hammerschmidt S. 2011. Impact of glutamine transporters on pneumococcal fitness under infection-related conditions. *Infect Immun* 79:44–58. <https://doi.org/10.1128/IAI.00855-10>.
68. Calder PC, Yaqoob P. 1999. Glutamine and the immune system. *Amino Acids* 17:227–241. <https://doi.org/10.1007/BF01366922>.
69. Castell LM, Bevan SJ, Calder P, Newsholme EA. 1994. The role of glutamine in the immune system and in intestinal function in catabolic states. *Amino Acids* 7:231–243. <https://doi.org/10.1007/BF00807699>.
70. Newsholme P, Curi R, Gordon S, Newsholme EA. 1986. Metabolism of glucose, glutamine, long-chain fatty acids and ketone bodies by murine macrophages. *Biochem J* 239:121–125. <https://doi.org/10.1042/bj2390121>.
71. Newsholme P, Gordon S, Newsholme EA. 1987. Rates of utilization and fates of glucose, glutamine, pyruvate, fatty acids and ketone bodies by mouse macrophages. *Biochem J* 242:631–636. <https://doi.org/10.1042/bj2420631>.
72. Costa Rosa LF, Cury Y, Curi R. 1991. Hormonal control of macrophage function and glutamine metabolism. *Biochem Cell Biol* 69:309–312. <https://doi.org/10.1139/o91-047>.
73. Wallace C, Keast D. 1992. Glutamine and macrophage function. *Metabolism* 41:1016–1020. [https://doi.org/10.1016/0026-0495\(92\)90130-3](https://doi.org/10.1016/0026-0495(92)90130-3).
74. Hava DL, LeMieux J, Camilli A. 2003. From nose to lung: the regulation behind *Streptococcus pneumoniae* virulence factors. *Mol Microbiol* 50:1103–1110. <https://doi.org/10.1046/j.1365-2958.2003.03764.x>.
75. Marra A, Asundi J, Bartilson M, Lawson S, Fang F, Christine J, Wiesner C, Brigham D, Schneider WP, Hromockyj AE. 2002. Differential fluorescence induction analysis of *Streptococcus pneumoniae* identifies genes involved in pathogenesis. *Infect Immun* 70:1422–1433. <https://doi.org/10.1128/iai.70.3.1422-1433.2002>.
76. Obert C, Sublett J, Kaushal D, Hinojosa E, Barton T, Tuomanen EI, Orihuela CJ. 2006. Identification of a candidate *Streptococcus pneumoniae* core genome and regions of diversity correlated with invasive pneumococcal disease. *Infect Immun* 74:4766–4777. <https://doi.org/10.1128/IAI.00316-06>.
77. Orihuela CJ, Gao G, Francis KP, Yu J, Tuomanen EI. 2004. Tissue-specific contributions of pneumococcal virulence factors to pathogenesis. *J Infect Dis* 190:1661–1669. <https://doi.org/10.1086/424596>.
78. Honsa ES, Johnson MD, Rosch JW. 2013. The roles of transition metals in the physiology and pathogenesis of *Streptococcus pneumoniae*. *Front Cell Infect Microbiol* 3:92. <https://doi.org/10.3389/fcimb.2013.00092>.
79. Manzoor I, Shafeeq S, Kuipers OP. 2015. Transcriptome analysis of *Streptococcus pneumoniae* D39 in the presence of cobalt. *Genom Data* 6:151–153. <https://doi.org/10.1016/j.gdata.2015.08.033>.
80. van Opijnen T, Camilli A. 2012. A fine scale phenotype-genotype virulence map of a bacterial pathogen. *Genome Res* 22:2541–2551. <https://doi.org/10.1101/gr.137430.112>.
81. Mina MJ, McCullers JA, Klugman KP. 2014. Live attenuated influenza vaccine enhances colonization of *Streptococcus pneumoniae* and *Staphylococcus aureus* in mice. *mBio* 5:e01040-13. <https://doi.org/10.1128/mBio.01040-13>.
82. Damjanovic D, Lai R, Jeyanathan M, Hogaboam CM, Xing Z. 2013. Marked improvement of severe lung immunopathology by influenza-associated pneumococcal superinfection requires the control of both bacterial replication and host immune responses. *Am J Pathol* 183:868–880. <https://doi.org/10.1016/j.ajpath.2013.05.016>.
83. Schmitz N, Kurrer M, Bachmann MF, Kopf M. 2005. Interleukin-1 is responsible for acute lung immunopathology but increases survival of respiratory influenza virus infection. *J Virol* 79:6441–6448. <https://doi.org/10.1128/JVI.79.10.6441-6448.2005>.
84. Blevins LK, Wren JT, Holbrook BC, Hayward SL, Swords WE, Parks GD, Alexander-Miller MA. 2014. Coinfection with *Streptococcus pneumoniae* negatively modulates the size and composition of the ongoing influenza-specific CD8<sup>+</sup> T cell response. *J Immunol* 193:5076–5087. <https://doi.org/10.1049/jimmunol.1400529>.
85. Shephardson KM, Larson K, Morton RV, Prigge JR, Schmidt EE, Huber VC, Rynda-Apple A. 2016. Differential type I interferon signaling is a master regulator of susceptibility to postinfluenza bacterial superinfection. *mBio* 7:e00506-16. <https://doi.org/10.1128/mBio.00506-16>.
86. Nakamura S, Davis KM, Weiser JN. 2011. Synergistic stimulation of type I interferons during influenza virus coinfection promotes *Streptococcus pneumoniae* colonization in mice. *J Clin Invest* 121:3657–3665. <https://doi.org/10.1172/JCI57762>.
87. Lee B, Robinson KM, McHugh KJ, Scheller EV, Mandalapu S, Chen C, Di YP, Clay ME, Enelow RI, Dubin PJ, Alcorn JF. 2015. Influenza-induced type I interferon enhances susceptibility to gram-negative and gram-positive bacterial pneumonia in mice. *Am J Physiol Lung Cell Mol Physiol* 309:L158–L167. <https://doi.org/10.1152/ajplung.00338.2014>.
88. Li W, Moltedo B, Moran TM. 2012. Type I interferon induction during influenza virus infection increases susceptibility to secondary *Streptococcus pneumoniae* infection by negative regulation of T cells. *J Virol* 86:12304–12312. <https://doi.org/10.1128/JVI.01269-12>.
89. Redford PS, Mayer-Barber KD, McNab FW, Stavropoulos E, Wack A, Sher A, O'Garra A. 2014. Influenza A virus impairs control of *Mycobacterium tuberculosis* coinfection through a type I interferon receptor-dependent pathway. *J Infect Dis* 209:270–274. <https://doi.org/10.1093/infdis/jit424>.



90. Högner K, Wolff T, Pleschka S, Plog S, Gruber AD, Kalinke U, Walmrath H-D, Bodner J, Gattenlöhner S, Lewe-Schlosser P, Matrosovich M, Seeger W, Lohmeyer J, Herold S. 2013. Macrophage-expressed IFN- $\beta$  contributes to apoptotic alveolar epithelial cell injury in severe influenza virus pneumonia. *PLoS Pathog* 9:e1003188. <https://doi.org/10.1371/journal.ppat.1003188>.
91. van Opijnen T, Boerlijst MC, Berkhout B. 2006. Effects of random mutations in the human immunodeficiency virus type 1 transcriptional promoter on viral fitness in different host cell environments. *J Virol* 80:6678–6685. <https://doi.org/10.1128/JVI.02547-05>.
92. Ho SN, Hunt HD, Horton RM, Pullen JK, Pease LR. 1989. Site-directed mutagenesis by overlap extension using the polymerase chain reaction. *Gene* 77:51–59. [https://doi.org/10.1016/0378-1119\(89\)90358-2](https://doi.org/10.1016/0378-1119(89)90358-2).
93. Horton RM, Cai ZL, Ho SN, Pease LR. 1990. Gene splicing by overlap extension: tailor-made genes using the polymerase chain reaction. *Biotechniques* 8:528–535.
94. Reed LJ, Muench H. 1938. A simple method of estimating fifty per cent endpoints. *Am J Epidemiol* 27:493–497. <https://doi.org/10.1093/oxfordjournals.aje.a118408>.